A Synergistic Analysis of Cloud Cover and Vertical Distribution from A-Train and Ground-Based Sensors over the High Arctic Station Eureka from 2006 to 2010

Yann Blanchard, Jacques Pelon, Edwin W. Eloranta, Kenneth P. Moran, Julien Delanoë, Geneviève Sèze

▶ **To cite this version:**

Yann Blanchard, Jacques Pelon, Edwin W. Eloranta, Kenneth P. Moran, Julien Delanoë, et al.. A Synergistic Analysis of Cloud Cover and Vertical Distribution from A-Train and Ground-Based Sensors over the High Arctic Station Eureka from 2006 to 2010. Journal of Applied Meteorology and Climatology, 2014, 53 (11), pp.2553-2570. 10.1175/JAMC-D-14-0021.1 . hal-01072075

HAL Id: hal-01072075
https://hal.science/hal-01072075

Submitted on 19 Nov 2020

HAL is a multi-disciplinary open access archive for the deposit and dissemination of scientific research documents, whether they are published or not. The documents may come from teaching and research institutions in France or abroad, or from public or private research centers.

L'archive ouverte pluridisciplinaire **HAL**, est destinée au dépôt et à la diffusion de documents scientifiques de niveau recherche, publiés ou non, émanant des établissements d'enseignement et de recherche français ou étrangers, des laboratoires publics ou privés.

A Synergistic Analysis of Cloud Cover and Vertical Distribution from A-Train and Ground-Based Sensors over the High Arctic Station Eureka from 2006 to 2010

YANN BLANCHARD AND JACQUES PELON

Laboratoire Atmosphères, Milieux, Observations Spatiales, UPMC-UVSQ-CNRS, Paris, France

EDWIN W. ELORANTA

Space Science and Engineering Center, University of Wisconsin–Madison, Madison, Wisconsin

KENNETH P. MORAN

Physical Sciences Division, NOAA/Earth System Research Laboratory, Boulder, Colorado

JULIEN DELANOË

Laboratoire Atmosphères, Milieux, Observations Spatiales, UPMC-UVSQ-CNRS, Paris, France

GENEVIÈVE SÈZE

Laboratoire de Météorologie Dynamique du CNRS, Ecole Polytechnique, Palaiseau, France

(Manuscript received 15 December 2013, in final form 4 June 2014)

ABSTRACT

Active remote sensing instruments such as lidar and radar allow one to accurately detect the presence of clouds and give information on their vertical structure and phase. To better address cloud radiative impact over the Arctic area, a combined analysis based on lidar and radar ground-based and A-Train satellite measurements was carried out to evaluate the efficiency of cloud detection, as well as cloud type and vertical distribution, over the Eureka station (80°N, 86°W) between June 2006 and May 2010. *Cloud–Aerosol Lidar and Infrared Pathfinder Satellite Observations* (*CALIPSO*) and *CloudSat* data were first compared with independent ground-based cloud measurements. Seasonal and monthly trends from independent observations were found to be similar among all datasets except when compared with the weather station observations because of the large reported fraction of ice crystals suspended in the lower troposphere in winter. Further investigations focused on satellite observations that are collocated in space and time with ground-based data. Cloud fraction occurrences from ground-based instruments correlated well with both *CALIPSO* operational products and combined *CALIPSO–CloudSat* retrievals, with a hit rate of 85%. The hit rate was only 77% for *CloudSat* products. The misdetections were mainly attributed to 1) undetected low-level clouds as a result of sensitivity loss and 2) missed clouds because of the distance between the satellite track and the station. The spaceborne lidar–radar synergy was found to be essential to have a complete picture of the cloud vertical profile down to 2 km. Errors are quantified and discussed.

1. Introduction

In the last decades, ground-based and satellite monitoring revealed that Arctic climate has undergone a substantial warming that is much larger than in other parts of the globe (Stocker et al. 2013). Ground-based measurements, in synergy with airborne and satellite data, show a persistent warming trend in the mean annual surface air temperatures of approximately 0.09°C $(10\,\mathrm{yr})^{-1}$ throughout the twentieth century (McBean et al. 2005). The warming is even more evident if one chooses to focus specifically on the measurements of the International Arctic Buoy Programme over the Arctic

Corresponding author address: Yann Blanchard, LATMOS, Boîte 102, Université Pierre et Marie, Curie, 4 place Jussieu, 75252 Paris CEDEX 05, France.
E-mail: yann.blanchard@latmos.ipsl.fr

DOI: 10.1175/JAMC-D-14-0021.1

© 2014 American Meteorological Society

Downloaded from http://journals.ametsoc.org/jamc/article-pdf/53/11/2553/3577679/jamc-d-14-0021_1.pdf by guest on 19 November 2020

Ocean, which showed a trend of 0.5°C $(10\,\mathrm{yr})^{-1}$ since 1979 (Rigor et al. 2000). During the same period, the September sea ice cover decreased at a rate of 12% $(10\,\mathrm{yr})^{-1}$ (Serreze and Barry 2011; Comiso 2012; Screen et al. 2012). To better understand the Arctic amplification process, certain feedbacks need to be better quantified. The surface energy budget is modulated by the change in surface albedo, the increased surface longwave emission due to the warmer surface, and the atmospheric feedback. Cloud formation and microphysical parameters also play a key role in the surface energy budget (Beesley 2000; Sedlar et al. 2012). For example, cloud occurrence and type are directly influenced by the change in sea ice area (Liu et al. 2012b) and air surface temperature (Eastman and Warren 2010a, hereinafter EW2010a). In fact, the decrease of sea ice extent and increase in sea surface temperature caused a positive regional trend of cloudiness, which is greater for low clouds (Kay et al. 2008). In addition, the total water vapor, which increases in the Arctic as the climate warms (Rinke et al. 2009; Serreze et al. 2012), has an impact on the cloud cover and leads to an increase in the warming of the lower troposphere.

Several ground-based stations were erected in the Arctic in the second half of the twentieth century, including weather stations. Despite their local nature, weather station observations can be subjective and are complicated by the lack of solar illumination during the winter period. Passive thermal infrared remote sensing instruments have been shown to improve cloud detection because they do not depend on the presence of the sun and can handle multiple particle layers. Since the 1970s, the advent of polar-orbiting satellite sensors allowed the estimation of the regional Arctic cloud cover (Curry et al. 1996; Serreze and Barry 2005). Polar cloud ''climatologies'' that are based on remote sensing measurements over the past decades have been made. Zonal studies show a disparity in annual cloud fraction in addition to monthly variations within the Arctic region (EW2010a; Shupe et al. 2011). Cloud cover is insufficient to describe cloud forcing, however, because intensive and extensive parameters such as cloud height, cloud optical depth, particle size, cloud temperature, and liquid water path have a direct impact on the shortwave and longwave fluxes (Dong et al. 2010). The identification of cloud type and phase (ice, liquid, or mixed phase) is of paramount importance as is cloud vertical distribution because of the induced radiative impact (Curry et al. 1996; Shupe and Intrieri 2004).

Active and/or passive instruments, operating in different parts of the electromagnetic spectrum, can be used to study cloud properties (see, e.g., Donovan and van Lammeren 2001; Delanoë and Hogan 2008). Depending on the instruments and analysis methods, Arctic cloudiness trends can lead to contradictory results in magnitude and even sign (Schweiger 2004; Y. Liu et al. 2010; Eastman and Warren 2010b, hereinafter EW2010b). These disparities can in part be explained by the differences in the satellite observational footprint and the variable sensitivity to certain types of clouds, sun-illumination conditions, and interferences with the underlying surfaces (Kahn et al. 2007; Kim et al. 2011; Chan and Comiso 2011). As a consequence, the extensive characterization of Arctic clouds necessitates an evaluation of the measurement methods and biases through comprehensive intercomparisons involving several complementing datasets, such as ground-based and satellite observations (i.e., measurements from below and above the cloud). Active satellite sensors are now available to retrieve vertically resolved cloud properties within a relatively small field of view that can be directly compared with ground-based coincident measurements (Kovacs and McCormick 2005; Kim et al. 2008).

In this paper, we focus on the synergistic use of lidar and radar data from the ground and from space so as to combine and assess their detection efficiency over the Eureka Arctic station. For the first time in the high Arctic, ground-based and spaceborne active instruments are compared on a statistical basis. The aim of this work is to identify and quantify their limitations so as to better infer cloud variations for climate studies. We first present the observations from active instruments (lidar and radar) as well as satellite and surface data. Statistical analyses that are based on independent datasets are summarized in a third section looking to annual, seasonal, and monthly variations of cloud occurrence. On the basis of the coincident data, joint statistics of cloud cover and vertical distribution are given in section 4. The section also highlights the limits of each observational dataset. We discuss results of the comparisons and identify biases and limitations (confirming some already identified). We also raise a few key points and questions about the use of these lidar and radar data in cloud climatology.

2. Observations and method

To analyze Arctic clouds we have used the largest common time series of several ground-based and satellite datasets to account for the diversity of events. In this part we present the instruments and analysis methods and also introduce used datasets.

a. The Eureka study site

Eureka is one of the northernmost sites in the Arctic that is equipped with a valuable suite of instruments to analyze cloud properties (see http://www.candac.ca for

Downloaded from http://journals.ametsoc.org/jamc/article-pdf/53/11/2553/3577679/jamc-d-14-0021_1.pdf by guest on 19 November 2020

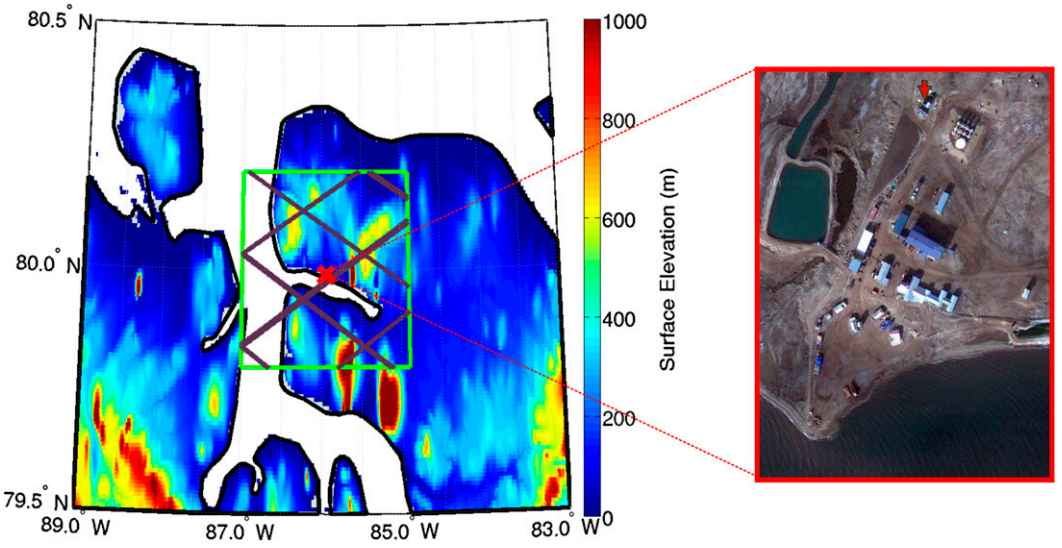

FIG. 1. A-Train tracks (in purple) close to the Eureka station (red X) during January 2007 (18 tracks), superposed over the digital elevation model Global 30 arc s elevation dataset (GTOPO30) used for *CALIPSO* data analysis. The green box (40 km × 40 km) delimits the area of this study. On the right-hand side an aerial view of the Eureka station shows that lidar and radar instruments are housed in two climate-controlled shipping containers (red arrow) 200 m north of the weather station.

an instruments inventory). The choice of a ground-based comparison site is limited in the high Arctic. In this work we used the following criteria: 1) frequent A-Train overpasses, 2) the longest available time series from active sensors since the launch of *Cloud–Aerosol Lidar and Infrared Pathfinder Satellite Observations* (*CALIPSO*) and *CloudSat* in the summer of 2006, 3) daily observations and measurements taken at a weather station, and 4) the availability of a long-term climatology. Only a handful of stations over the polar circle satisfy these criteria, namely, Ny Alesund, Barrow, and Eureka. Given the time series and the instrument performances, we chose the Eureka station (79°59′N, 86°56′W; Nunavut, Canada), situated in the Canadian Archipelago, to conduct this study. Figure 1 shows the location of the Eureka station and the position of the selected box for which the spaceborne observations are considered in this study. Located close to the A-Train latitude limit of 82°N, it offers the opportunity of a larger number of overpasses, with a monthly average of 16 overpasses within less than 28 km of the station. A zoom over the location (Fig. 1) shows examples of *CALIPSO* overpasses that are close to Eureka during one month. In a year, the maximum standard deviation in distance of the same track (occurring every 16 days) is about 2.03 km. The size of the box was chosen to contain a maximum of overpasses while trying to avoid potential orographic effects in this fjord region where the ground level varies from 0 to 1.2 km above sea level. The latter choice was done according to the criteria of Kovacs and McCormick (2005). They suggest, for cloud-comparison purposes, a length scale of a few tens of kilometers and a time scale of a few minutes.

In the framework of the Study of Environmental Arctic Change (SEARCH) and the Canadian Network for the Detection of Atmospheric Change (CANDAC), a lidar and a radar (described later in this section) were continuously operating from the summer of 2005 until 2010 (http://lidar.ssec.wisc.edu/syst/ahsrl/ahsrl_data.htm). The Eureka weather station (operating within the mandate of Environment Canada) has been providing hourly data of surface air temperature, pressure, humidity, wind, and weather observations since 1953. Radiosondes have also been launched 2 times per day since 1948, but humidity profiles are available only since 1972 (downloaded from the Integrated Global Radiosonde Archive website: http://www.ncdc.noaa.gov/oa/climate/igra/index.php). The instruments and datasets used in this study are summarized in Table 1 and will be described in the next sections.

b. *Meteorological observations at Eureka*

Standard surface measurements are accompanied by visual sky observations several times per day. This task is performed by an operator and depends on sites and procedures. At Eureka, observations are reported hourly and give information on cloud presence and visibility. There are, however, major issues linked to the lack of illumination during the winter. Several authors discussed biases caused in cloud amounts observed from

Downloaded from http://journals.ametsoc.org/jamc/article-pdf/53/11/2553/3577679/jamc-d-14-0021_1.pdf by guest on 19 November 2020

TABLE 1. Instruments and datasets used in this study.

	Ground based	On board satellite	Information retrieved
Weather data	Radiosonde and weather station observations (Environment Canada)	Global Modeling and Assimilation Office reanalysis under the *CALIPSO* track (from *CALIPSO* data)	Atmospheric profiles
Lidar	AHSRL (Eloranta 2005)	CALIOP level-2 cloud and aerosol layer (Winker et al. 2009)	Atmospheric feature: cloud/aerosol/clear sky; depolarization
Radar	MMCR (Moran et al. 1998)	*CloudSat* level-2 cloud mask (GEOPROF) and precipitation (Stephens et al. 2002)	Precipitation; cloud phase
Synergy lidar–radar	(Donovan and van Lammeren 2001; Shupe 2007)	DARDAR mask (Delanoë and Hogan 2010)	Pixel classification profile (combining lidar and radar performances); cloud microphysical properties
Ancillary data	Microwave radiometer (Turner et al. 2007)	IIR level 2 (Garnier et al. 2012), MODIS (MYD/MOD08_D3 and _M3), AVHRR (APPx DATA 025KM)	Liquid water content; scene classification; opacity; cloud fraction from passive instruments

the surface during polar night (Hahn et al. 1995) and proposed to keep only observations occurring with sufficient moonlight. In winter another issue occurs when ice crystals suspended in the lower troposphere (reported as ''ice crystals'') mask upper features. Ground-based weather observations may also be subject to local bias (e.g., orographic effects) and may not be representative at the regional scale. The inadequate geographic coverage is problematic in a region where interannual variations are not uniform over land and ocean, depending on the latitude (Shupe et al. 2011). In our study, we used all ground-based observational data without any masking.

c. *Ground-based active instruments*

Measurements from the Arctic high-spectral-resolution ground-based lidar (AHSRL) developed by the University of Wisconsin (Eloranta et al. 2007) were used in this study (see Table 1). Retrieved particulate backscatter profiles at 532 nm indicate the presence and the altitude of particles, as long as the lidar signal is not attenuated by opaque clouds. Combined with the lidar depolarization ratio, backscatter profiles are used to distinguish the presence of clear-sky, ice or liquid particles and aerosols. Data from the Eureka high-frequency cloud radar (Moran et al. 1998) are also used for cloud characterization. Because radar reflectivity is proportional to the sixth power of the hydrometeor diameter and to the fourth power of the frequency (this approximation is valid while the radar frequency and the particle sizes are small enough to be considered to be in the Rayleigh scattering regime), the Eureka radar [frequency $f = 35$ GHz; wavelength $\lambda = 8.7$ mm for the millimeter-wavelength cloud radar (MMCR) in Table 1] is thus ideal for precipitation and clouds studies. Correlatively, the radar may miss cloud droplets and the associated warm clouds and underestimate elevated cold cloud-top altitude where small ice particles can be found. Because this MMCR is Dopplerized, we also used velocity and spectrum-width fields to help to discriminate among ice, liquid, or mixed-phase clouds (Shupe and Intrieri 2004). Atmospheric profiles from rawinsondes give the temperature profile and, hence, the cloud-layer inner temperature. The 0°C threshold is used to distinguish between rain and snow precipitation, and −40°C indicates the homogeneous freezing point below which hydrometeors are considered to be ice.

The ground-based multisensor pixel classification applied in this work is based on Shupe (2007) because we use the same instruments at the same ground site. Each pixel (for 30-m vertical and 10-s temporal resolutions) is first classified as one of the atmospheric features using a lidar mask. The radar cloud measurements then help to identify the cloud phase or precipitation type. For opaque cloud where the lidar signal is extinguished, radar data can extend the classification of upper pixels. A coherence filter (7×7 pixels) is then applied to avoid false-alarm pixels and to homogenize the classification. The choice of the fixed thresholds between the different classes, which is based on 7 years of observations (Shupe 2007), may, however, lead to wrong classification, as in, for example, an underestimation of snow precipitation in winter (on the basis of a comparison with ground weather observations; not shown here). Pixels classified as snow were gathered with ice, and those classified as rain and drizzle were gathered with liquid water. Cloud-occurrence

Downloaded from http://journals.ametsoc.org/jamc/article-pdf/53/11/2553/3577679/jamc-d-14-0021_1.pdf by guest on 19 November 2020

fraction, hereinafter referred to as cloud fraction, is the amount of time that clouds are present and detectable by the remote sensing instruments and, for active instruments, is obtained from the analysis of the vertical classification. To avoid false cloud detection, we required that a cloud layer should have a vertical extent that is equal to or higher than 90 m (3 pixels). In the text and figures, the result of the classification that uses the synergy of ground-based lidar and radar at Eureka is named EUREKA_G/B. Ground-based data availability is limited to the period 2005–10 for the lidar and the radar. Failures and maintenance—mainly done in summer—also restrict good-quality measurements and may alter annual statistics. Indeed, Protat et al. (2006) advocate that time-based sampling variations (e.g., due to maintenance or failures) of ground-based measurements may lead to some differences in cloud fraction.

d. Satellite observations

1) PASSIVE SATELLITES

Visible and thermal infrared satellite instruments [e.g., the Television and Infrared Observation Satellite (TIROS) Operational Vertical Sounder (TOVS) or Advanced Very High Resolution Radiometer (AVHRR)] enabled a global picture of Arctic clouds (Schweiger et al. 2008; EW2010b). These passive instruments, however, are known to suffer from several limitations in the Arctic, such as the absence of sunlight during the polar winter, the cold surface temperature, the inversion layer, and the albedo of snow surfaces (Lubin and Morrow 1998; Y. Liu et al. 2010). When compared with ground-based observations, these sensors showed different monthly averages and long-term trends (Wang and Key 2005; EW2010b). Moreover, because of technical limitations, some crucial cloud information cannot be retrieved, such as cloud-base altitude, particle phase, or presence of precipitation. The use of active instruments, which emit their own radiation, can help to obtain these missing pieces of information. In some specific cases, however (e.g., very low clouds over vegetated areas during daytime), passive sensors [like the Moderate Resolution Imaging Spectroradiometer (MODIS); see Table 1] could help in detecting cloud structures that active instruments have difficulties detecting (Chan and Comiso 2011).

2) ACTIVE SENSORS AND NEW A-TRAIN DATASETS

CALIPSO and *CloudSat*, which are part of the Afternoon Train (or A-Train) satellite constellation (Stephens et al. 2002), helped to significantly improve the study of polar clouds. The satellites' polar orbit allows overpasses between 82°N and 82°S with unprecedented horizontal resolution [from 0.33 to 1 km for Cloud-Aerosol Lidar with Orthogonal Polarization (CALIOP) and 1.4 km for *CloudSat* cloud profiles] and vertical resolution (from 30 to 60 m for CALIOP and 500 m for *CloudSat*). A-Train satellites provide frequent active measurements in the Arctic, which are spatially extended by such passive instruments as the infrared imaging radiometer (IIR) on *CALIPSO* (Winker et al. 2009) or MODIS on *Aqua* (Platnick et al. 2003). CALIOP measures the backscatter cross section at two wavelengths (532 and 1064 nm) with two polarizations at 532 nm (Winker et al. 2003). Aerosol or cloud-layer detection is done using a threshold on the attenuated scattering ratio vertical profiles (Vaughan et al. 2009). The *CloudSat* radar has a frequency of 94 GHz, whereas MMCR is a 35-GHz-frequency radar. For radars with the same resolution volume and transmitted power, the radar with the shorter wavelength (i.e., higher frequency) is capable of detecting smaller particles (Lhermitte 1987). It should nevertheless be considered that *CloudSat* has a lower sensitivity (minimum detectability of −30 dBZ) than the ground-based radar [between −49 and −30 dBZ at 5 km, depending on the operating mode (Moran et al. 1998)]. Previous comparisons between MMCR (at Darwin, Australia) and *CloudSat* showed an overall good agreement in terms of statistical reflectivity profiles (Protat et al. 2009; Z. Liu et al. 2010). This limit of detectability of ice particle diameter is about 40 μm, and it depends on the particle number concentration (Grenier et al. 2009) and affects cloud-detection performances (Stephens et al. 2002). The *CloudSat* cloud mask is a value given as an indicator of the cloud-detection probability (40 being the highest value for cloud-detection probability higher than 99.8%). In this study, we use CALIOP level-2, version 3, layer products, which provide altitudes and type of cloud or aerosol layers, and *CloudSat* level-2 products, which provide altitudes of cloud as well as the type of precipitation. We also employed the radar–lidar (DARDAR) mask (version 1.1.4) in our comparison study because it uses a comprehensive synergy of CALIOP and *CloudSat* (Delanoë and Hogan 2010). *CALIPSO* also carries a three-channel IIR that measures radiances at 8.65, 10.6 and 12.05 μm with 1-km horizontal resolution over a 69-km swath. IIR swath data (version 3) were used as a means to evaluate the extension of the IIR classification on the track using CALIOP classification in the IIR pixels from radiatively equivalent pixels (Garnier et al. 2012). The IIR swath product is used here to analyze cloud detection over the box. For each overpass, we extracted the pixels in the 40 km × 40 km box and used their scene classification to derive cloud fraction, by keeping the dominant type.

Downloaded from http://journals.ametsoc.org/jamc/article-pdf/53/11/2553/3577679/jamc-d-14-0021_1.pdf by guest on 19 November 2020

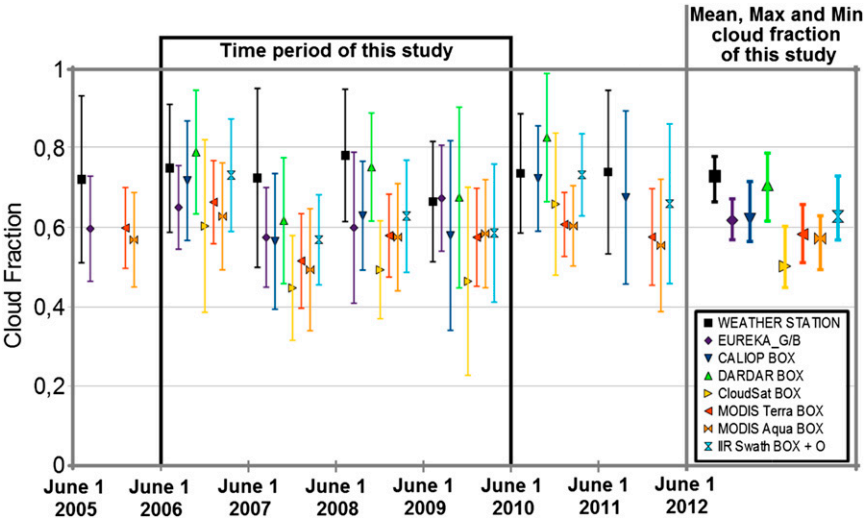

FIG. 2. Annual cloud fraction and standard deviation for the datasets presented in Table 1 for the period June 2005–June 2012.

e. Synergetic observations and trends

Meteorological observations and spaceborne passive measurements such as AVHRR have been performed over decades, and long-term trends have been analyzed in various papers (EW2010b). We have looked at the context offered by such long-time-series space observations at Eureka. It is not our objective, however, to detail here these analyses because the paper focuses on more recent active observations. Detailed results are reported in appendix A. Looking at the cloud fraction, it is seen that a good coherence is observed between MODIS and AVHRR, with an overall decrease in cloud fraction. However, from the ground-based observations for skies that are other than clear (see Fig. A1 in appendix A), although the agreement was good with satellite data in the 1980s we find opposite trends between spaceborne and ground-based observations, leading to an increased difference in the last years. These results emphasize the need to go into further detail in the analysis and look at additional data. To do so, we focus in the next sections on the more recent datasets from the A-Train.

3. Statistics from independent recent datasets

a. Comparison of annual cloud fraction from independent datasets

To intercompare cloud fraction measurements, we compiled the available data from observations, active instruments, and passive instruments. Figure 2 displays the cloud fractions and standard deviations from the various datasets gathered for a period covered by both ground-based and satellite active sensors, extending from June 2005 to June 2012.

The weather-station cloud fraction, named total nebulosity, merged all non-clear-sky observations where "clouds," "ice crystals," and "snow" observations represent 96%. The total nebulosity is expected to overestimate the cloud fraction because ice-crystals events can also happen during clear sky (Intrieri and Shupe 2004). The measurement statistics include hourly observations from the weather station and hourly profiles from ground-based lidar and radar instruments (for long-term statistics we took a 1-h temporal resolution). A-Train data (CALIOP, DARDAR, *CloudSat*, and IIR) were extracted whenever available. The term "box" means that we calculated the cloud fraction among all of the profiles over the 40 km × 40 km box centered over Eureka as shown in Fig. 1. MODIS annual means were extracted and averaged over Eureka from monthly data with a 1° × 1° resolution.

In the time period considered in Fig. 2, the annual cloud fraction values are between 0.45 and 0.82. All satellite data except the DARDAR ones agree better with EUREKA_G/B—with an average value of ~0.62—than with weather station data (closer to DARDAR)—with an average value of ~0.73. The interannual variations are very small (less than 0.1), but no significant trend can be extracted over such a short period.

CALIOP is supposed to be sensitive to all types of clouds, but Chan and Comiso (2011) show that certain lower-tropospheric clouds near the surface can be missed by CALIOP. Low clouds are also an issue in *CloudSat* data because of the ground clutter impact up to 1 km above the surface (Tanelli et al. 2008). The DARDAR cloud mask, which combines information

Downloaded from http://journals.ametsoc.org/jamc/article-pdf/53/11/2553/3577679/jamc-d-14-0021_1.pdf by guest on 19 November 2020

TABLE 2. Seasonal means of cloud fraction over the Eureka station derived from different datasets (standard deviations in parentheses) for the period 1 Jun 2006–31 May 2010, except for Shupe et al. (2011) (between 2005 and 2009).

	Instruments	JJA	SON	DJF	MAM
Ground-based	Weather station	0.60 (0.12)	0.76 (0.04)	0.86 (0.12)	0.69 (0.08)
	EUREKA_G/B	0.52 (0.12)	0.74 (0.02)	0.67 (0.04)	0.57 (0.09)
	Radar–lidar: Shupe et al. (2011)	0.58	0.74	0.72	0.61
Satellite	MODIS (MYD08 M3 and MOD08 M3)	0.64 (0.07)	0.69 (0.04)	0.51 (0.07)	0.47 (0.07)
	DARDAR BOX ALL	0.66 (0.19)	0.87 (0.06)	0.69 (0.05)	0.62 (0.06)
	DARDAR BOX HIGH	0.65 (0.20)	0.83 (0.07)	0.58 (0.12)	0.50 (0.05)
	CALIOP BOX	0.61 (0.15)	0.75 (0.02)	0.65 (0.07)	0.48 (0.07)
	IIR SWATH BOX + O	0.62 (0.16)	0.73 (0.04)	0.64 (0.07)	0.53 (0.05)
	CloudSat BOX	0.51 (0.16)	0.63 (0.08)	0.44 (0.07)	0.43 (0.04)
	CloudSat BOX 2	0.55 (0.13)	0.66 (0.08)	0.51 (0.08)	0.48 (0.04)

from *CALIPSO* and *CloudSat* cloud masks, tends to overestimate cloud fraction relative to that seen in other datasets at Eureka. We notice that DARDAR data often give a small layer of supercooled droplets near the ground because of the ground backscatter of the radar signal. The cloud-fraction differences in passive instruments (MODIS and IIR) are due to the cloud-detection methods, since IIR is used to extend CALIOP cloud detection along track through its swath. The IIR algorithm is not able to classify some pixels; this scene type is identified as "others" (O). Indeed, some very thin clouds (mainly high clouds, which require a horizontal averaging of 80 km) are not taken into account in the present IIR classification (Garnier et al. 2012). A careful look at these latter scenes using CALIOP data shows that these pixels mostly correspond to mixed types including clouds. Consideration of all of these pixels (in the IIR SWATH + O) would lead to an increase of ~6%. MODIS detects a smaller cloud fraction because of certain limitations when over the Arctic environment, as described in section 2d. There can be errors that are caused by interferences in the cloud detection with ice cover (Y. Liu et al. 2010). Because of the absence of solar illumination during winter, standard cloud-detection techniques have been modified to reduce misidentifications (Liu et al. 2004). MODIS overpass time over Eureka (around 0030 and 2000 UTC for *Terra* and 1100 and 1530 UTC for *Aqua*) has a real but negligible impact on cloud fraction in comparison with the other standard deviations and variability.

Figure 2 shows that instrument characteristics or the methods themselves can lead to some differences, as with active and passive sensors over Eureka. For another Arctic ground site (Barrow), ground-based results compiled by Dong et al. (2010) confirm that discrepancies in cloud detection can originate from the measurement methods, the instrumentation suite, or the time period. These heterogeneities, combined with the small number of Arctic stations, can explain the limits of using the ground-based databases to define a regional trend. Satellite active measurements have advantages that seem to be helpful. The need of satellite measurements to have a regional coverage is nevertheless contrasted by the performances of the different sensors and their relatively small lifetime. It is, however, possible to go further in the analysis, looking to seasonal variations to highlight instrument efficiencies.

b. *Seasonal and monthly cloud fraction over Eureka*

A seasonal analysis of cloud fraction reveals some specific disparities over certain periods of the year and can be analyzed in the context of recent polar cloud climatologies (e.g., Liu et al. 2012a). For this section we focused on the period 1 June 2006–31 May 2010 (see Fig. 2), for which most of the datasets were available. Data from 546 A-Train tracks and more than 30 000 hourly observations from the weather station and vertical profiles from EUREKA_G/B active instruments were used in creating Table 2. It summarizes seasonal cloud fraction obtained in this study for the datasets over Eureka, including a comparison with the previous study of Shupe et al. (2011). MODIS gathers monthly data from *Terra* and *Aqua*. DARDAR "BOX HIGH" corresponds to DARDAR "BOX ALL" except that the first two pixels over the ground (120 m) are removed as possibly contaminated by the ground return of the radar signal. *CloudSat* "BOX 2" is *CloudSat* "BOX" combined with the weak-cloud detection using along-track integration (cloud mask value between 6 and 10). IIR SWATH BOX + O means that the scenes classified as O by IIR are reclassified as clouds on the basis of a comprehensive comparison with CALIOP observations (see previous section).

As shown in Table 2 and in Liu et al. (2012a) over the Canadian Arctic Archipelago, the autumn period (September–November) is characterized by the highest overall cloud fraction (~0.74). For the weather station, the maximum is much larger and is observed later in the winter because of the "ice crystals" observations that may

Downloaded from http://journals.ametsoc.org/jamc/article-pdf/53/11/2553/3577679/jamc-d-14-0021_1.pdf by guest on 19 November 2020

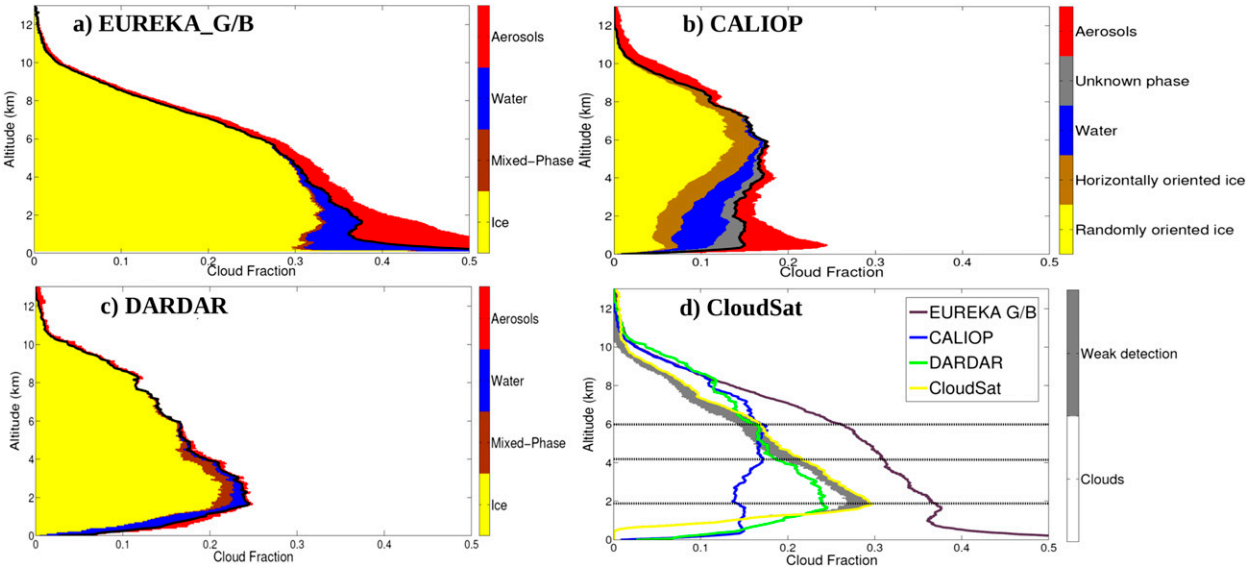

FIG. 3. Cumulated vertical scene-type distribution between June 2006 and May 2010 for all of the active instruments: (a) EUREKA_G/B, (b) CALIOP, (c) DARDAR, and (d) *CloudSat*. The black lines in (a)–(c) correspond to the cloud-only vertical distribution. They are redrawn and colored in (d) for comparison purposes.

be part of low-level haze (see appendix A). The least cloudy season is March–May (MAM), with cloud fraction of approximately 0.50 associated with large standard deviations, as a result of high interseasonal variations. This is in agreement with the transition from polar winter minimum of cloud fraction to summer (Beesley and Moritz 1999; Y. Liu et al. 2010). The comparison between the EUREKA_G/B cloud fractions and those from Shupe et al. (2011) shows some discrepancies that are most probably caused by the difference in temporal resolution (1 h vs 30 s) combined with the coherence filter (Shupe 2007), which removes short-lifetime and sparse clouds. Moreover, the time period considered here is different (2006–10 vs 2005–09).

Additional results are presented in appendix B that show (see Fig. B1) that ground-based and satellite data yield similar trends, except during the months in which the missing Eureka data (from lidar failures and maintenance) bias EUREKA_G/B statistics.

c. *Cloud-type distribution*

In addition to the seasonal variations, cloud-fraction differences among active instruments can originate from detection problems in the vertical direction. We thus looked at the type of particles identified by the different active instruments along the vertical profiles between June 2006 and May 2010. (This set corresponds to the same number of observations that were used in Table 2 and in Fig. B1 of appendix B.) Figure 3 gives the vertical distributions decomposed as a function of the following classes: aerosols (detected by lidar only), water, ice (horizontally and randomly oriented), mixed-phase clouds, and unknown-phase clouds. The black lines on each figure correspond to the cloud vertical profile. For discussion purposes, EUREKA_G/B, CALIOP, and DARDAR cloud vertical profiles are superimposed with the *CloudSat* one in Fig. 3d.

The comparison of the vertical cloud distributions reported in Fig. 3d shows that the cloud detection of the spaceborne lidar is the most efficient down to an altitude of ~6 km, at which limitations in the detection could be induced by the attenuation of optically dense clouds. The number of the detected ice particles indeed decreases below 6 km, whereas the presence of liquid particles increases. CALIOP and *CloudSat* appear to have a similar sensitivity to clouds at 6 km. *CloudSat* measurements are very sensitive to clouds below 4 km but miss high thin ice clouds above 6 km and everything below 0.8 km because of the ground clutter. Indeed, to avoid false detection, pixels corresponding to several hundred meters above the ground are not to be used in the *CloudSat* cloud detection (Tanelli et al. 2008). The weak-cloud detection (using along-track integration) increases the cloud vertical profile by a few percent and is more often used for medium and high clouds where the particle size is often smaller. It may, however, lead to wrong detection, as discussed in appendix B. DARDAR observes a majority of ice particles except in the first hundred meters where supercooled and liquid droplets are identified as mentioned in the previous section.

Downloaded from http://journals.ametsoc.org/jamc/article-pdf/53/11/2553/3577679/jamc-d-14-0021_1.pdf by guest on 19 November 2020

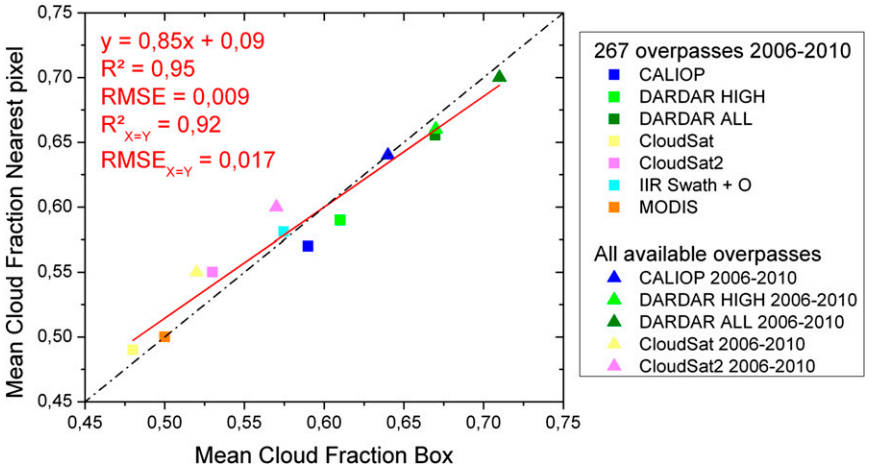

FIG. 4. Mean cloud fraction of the nearest pixel and of the box for various datasets showing a maximal difference of 3% between the "box" and the "nearest" mean cloud fractions. Dash–dotted line represents 1:1 correspondence.

CALIOP also detects aerosols close to the ground as well as above the tropopause. Those two aerosol domains are in agreement with the CALIOP extinction profiles observed in the whole Arctic between 2006 and 2010, when few volcanic eruptions occurred (Di Pierro et al. 2013). The stratospheric aerosols seen by CALIOP are also seen, to a lesser extent, by EUREKA_G/B but are considered to be clouds by DARDAR.

In Fig. 3d we have identified a lower level, marked by the first dashed line at 1.9 km, below which the influence of the surface appears to be more predominant and causes large discrepancies among datasets. In this low layer, atmospheric features cannot be well detected from space, and the occurrence of aerosols, ice, and water particles is underestimated when compared with EUREKA_G/B. Figure 12b in Shupe et al. (2011) confirms that the cloud-base heights from ground-based measurements are more frequently located in the first 2 km, except in summer when a decrease in low-level moisture is observed.

The independent datasets represent a large amount of data. They suffer from a lack of time representativeness, however. On the one hand, instrument failures (i.e., in the summers of 2006 and 2008 and in the spring of 2010 for EUREKA_G/B) and local effects (i.e., ice crystals) may enhance specific cloud features. These thus lead to specific occurrence differences in altitude, biasing the comparisons. On the other hand, the times of A-Train overpass (~1100 and 1530 UTC) do not allow one to describe fully the cloud diurnal cycle, even if the differences in the cloud vertical profile seem to be negligible (according to a similar analysis made while keeping only A-Train overpass times).

4. Analysis of coincident observations

To carry out a more representative comparison between the observations from the selected instruments, we chose to restrict the database to data from times when all instruments were correctly and simultaneously operating. This criterion resulted in 267 coincident overpasses over the 40 km × 40 km box centered on Eureka (see Fig. 1).

For all satellite datasets used in this section, Fig. 4 shows the comparison between the mean cloud fractions of the nearest pixels to Eureka and the mean value averaged over the box. The obtained correlation R is relatively high, with a value $R^2 = 0.95$ and a dispersion of about 2% with respect to a 1:1 line, which is within the uncertainties. Chi-square tests show, moreover, that there is no significant difference, for the same dataset, between mean cloud fractions from nearest profiles and from the box. The latter result allows us to keep only the nearest satellite vertical profiles to compare with ground-based profiles at the same time, given the time step of 10 s.

a. Cloud detection of A-Train coincident overpasses over Eureka

To analyze the cloud-detection efficiency using coincident measurements, we compare CALIOP, IIR, DARDAR, and *CloudSat* detection of cloudy and clear scenes, considering EUREKA_G/B as the reference. As in section 3, IIR SWATH BOX + O data were used to get a complete view of the box, where the dominant type was kept to derive cloud fraction. Results are reported in Table 3.

Downloaded from http://journals.ametsoc.org/jamc/article-pdf/53/11/2553/3577679/jamc-d-14-0021_1.pdf by guest on 19 November 2020

TABLE 3. Cloud-detection statistics among the nearest profiles of the 267 overpasses from spaceborne datasets in comparison with ground-based lidar–radar measurements. The percentage of the number of cases appears in parentheses. The cloud fraction and the total hit rate for each comparison between satellite and ground-based observations is also given.

		CALIOP		IIR SWATH + O		DARDAR		*CloudSat*		Cloud fraction
		No Cloud	Cloud	No Cloud	Cloud	No Cloud	Cloud	No Cloud	Cloud	
EUREKA_G/B	No Cloud	89 (33)	9 (3)	91 (34)	7 (3)	74 (28)	24 (9)	86 (32)	12 (4)	63.3
	Cloud	27 (10)	142 (53)	21 (8)	148 (55)	18 (7)	151 (57)	49 (18)	120 (45)	
Cloud fraction (%)		56.6		58.1		65.5		49.4		
Hit rate (%)		86.5		89.5		84.3		77.2		

These 267 overpasses are not expected to be representative of the cloud statistics over Eureka because of the time sampling. Cloud fractions obtained for these coincident overpasses are somewhat different than those derived from independent statistics (see Fig. 2 for the period 2006–10) for CALIOP and DARDAR (approximately −5%) but agree for the other datasets. Table 3 corroborates that CALIOP and EUREKA_G/B have a relatively good correlation (231 good detection cases from 267 tracks, which represents a hit rate of ~86.5%). It is almost 90% for IIR and close to 85% for DARDAR, but, as expected from previous comparisons, the *CloudSat* hit rate remains smaller (77%). Since the lidar is sensitive to small particles, one expects that both ground-based and satellite instruments can detect a cloud when it occurs. In some cases, however, clouds are misclassified as aerosols (in about one-third of CALIOP wrong detections) and can even go undetected as a result of the thresholds associated with classification methods. Clouds appear to be better detected by IIR SWATH BOX. This result is due to the representativeness of observations with respect to cloud heterogeneity, which is better accounted for using the IIR swath. When only the nearest pixel over Eureka from IIR SWATH BOX is used, the hit rate decreases to 82.7% however. This surprising result is due to the variability of the surface type for the closest pixels surrounding the station, which has an impact on the surface emissivity and then on the computation of the radiatively equivalent pixels (Garnier et al. 2012).

The latter comparison suffers from not accounting for a scene-representativeness factor, which is the distance between Eureka and the nearest pixel. By analyzing the CALIOP hit rate as a function of the distance, we concluded that pixels that are closer than 5 km detect the same features as EUREKA_G/B with 95% confidence. This rate decreases, and toward the edge of the box (more than 20 km away from the station) the hit rate is about 80%. We will, however, be obliged to consider all 267 profiles in order to keep enough data. We do have to keep in mind that in certain scenes the instruments are not looking at the same features, and that situation leads to misidentifications.

b. *Cloud vertical distribution*

The cloud detection is not sufficient to conclude whether the features are detected at the same altitude. Cloud vertical distribution is an important parameter in the comparison to focus upon, because it helps to determine cloud radiative forcing. We calculated the vertical cloud fraction for EUREKA_G/B, CALIOP, DARDAR, and *CloudSat*, as done in section 3c, but for the coincident profiles. Results are reported in Fig. 5.

Cloud-fraction profiles reported in Fig. 5a are very similar to the vertical profiles of Fig. 3d for the spaceborne observations. EUREKA_G/B shows, however, a consistently lower cloud fraction than in the previous independent analysis because of a different sampling. In Fig. 5a the EUREKA_G/B results appear to be in very good agreement with DARDAR and *CloudSat* for medium and low clouds, except for the very low clouds. Temperature profiles (Fig. 5b) show that the uppermost altitude for the tropopause is observed at 10.9 km, which corresponds to the top altitude of the upper clouds detected. Because all spaceborne observations are colocalized, the radar nondetection implies that a large part of high clouds are thin cirrus with small ice particles. EUREKA_G/B synergy also detects fewer high clouds than DARDAR or CALIOP because of lower thick clouds. The homogeneous freezing at −40°C may appear as low as 5 km but is at 6 km on average. This means that all of the atmospheric features above this limit are supposed to be ice. According to CALIOP, the opaque-cloud vertical profiles show that 14% of the 267 coincident overpasses (or 25% of the cloudy profiles) are considered to be opaque. This number is, however, much lower if we consider IIR with a threshold on the effective emissivity at 12 μm (i.e., $\varepsilon > 0.95$).

Midlevel clouds are almost detected similarly by all instruments. In the bottom of the domain, CALIOP shows a deficiency in cloud detection, which is accentuated at lower altitudes. This is explained by the fact that cloud opacity occurrence is increasing as altitude decreases below 8 km but, more important, below 5 km

Downloaded from http://journals.ametsoc.org/jamc/article-pdf/53/11/2553/3577679/jamc-d-14-0021_1.pdf by guest on 19 November 2020

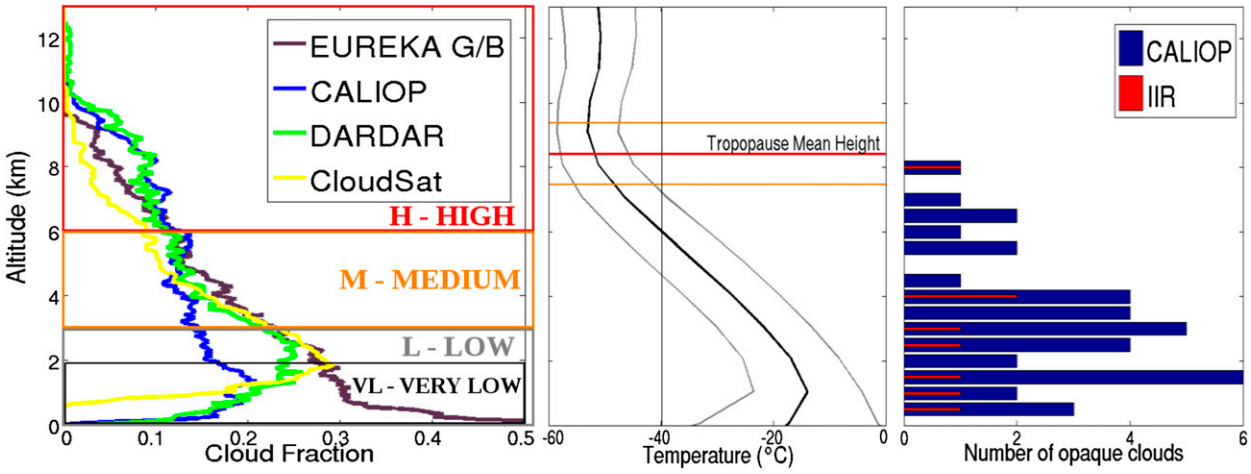

FIG. 5. (a) Vertical distribution of the cloud fraction per bin obtained from the active instruments for the 267 nearest overpasses of A-Train over Eureka, (b) mean temperature profile (±1 std dev shown by thin gray lines) as well as tropopause mean height (±1 std dev shown by thin orange lines), and (c) number of opaque clouds according to CALIOP opaque flag and IIR emissivity. The vertical distribution of the cloud fraction per altitude bin has been divided in the three vertical domains defined by the International Satellite Cloud Climatology Project (Rossow and Schiffer 1991), with limits at 440 and 680 hPa. In the low-cloud domain (pressure above 680 hPa), we added a very-low-cloud domain (VL) close to the surface (for $P > 830$ hPa or $z < 1.9$ km).

(Fig. 5c). Supercooled droplets in water or mixed-phase clouds are rapidly attenuating lidar signals. They happen when temperatures are higher than −40°C, before the homogeneous freezing occurs. As shown by Fig. 5b, this happens below 5 km, that is, in the lower part of the midlevel clouds. This result may explain the decreasing detection efficiency of CALIOP as observed with respect to the other instruments. On the contrary, *CloudSat* and DARDAR detect more clouds since the radar is sensitive to thick clouds with large particle size, as in mixed-phase and precipitating clouds.

Low clouds [pressure $P > 680$ hPa; i.e., altitude $z <$ 2.7–3.3 km, in the "low" (L) section of Fig. 5a] appear to be the dominant feature in the vertical cloud distributions, as observed in EW2010a and in Liu et al. (2012b), whatever the sensors. Nevertheless, there are some discrepancies with regard to the cloud fraction. As discussed before, CALIOP is shown to have a much weaker sensitivity to low-level structures. When low-altitude clouds are dense clouds, sometimes precipitating, the spaceborne lidar is able to detect only the upper limit of such structures. Furthermore, because of attenuation during propagation reducing the signal-to-noise ratio, it may not detect semitransparent ones below (e.g., haze). As mentioned before, above 1.9 km, *CloudSat* and EUREKA_G/B show almost the same cloud occurrences.

The main difference in this comparison happens for very low clouds [in the "very low" (VL) section of Fig. 5a]. We know that these clouds may be difficult to detect from space over complex terrain (inhomogeneities; signal perturbations). EUREKA_G/B has a very high cloud fraction in the first 100 m, often associated with small optical depth. This is most probably due to local effects and the presence of ice crystals close to the ground that were classified as a cloud. As opposed to that, the *CloudSat* and DARDAR cloud fractions quickly decrease below 1 km, where ground clutter affects the radar backscatter. Because of this limitation, CALIOP and DARDAR have almost the same profiles where cloud fraction decreases from 0.2 (at 1 km) to 0 (at the surface), possibly underestimating the cloud fraction as discussed above. Indeed, about 65% of misdetection in Table 3 is due to low clouds (with a cloud-top pressure above 680 hPa).

From this comparison, we conclude that only DARDAR is able to detect the cloud profile with relatively good agreement with ground-based measurements. Below 1 km, occurrences of low cloud or ice crystals are not captured well by spaceborne instruments when EUREKA_G/B is used as the reference.

c. *Seasonal cloud vertical distribution*

Although the total number of selected cases is low, a tentative analysis is performed to look at seasonal behavior. The vertical profiles of Fig. 5a are seasonally decomposed to analyze their differences.

Figure 6 confirms the good agreement between ground-based observations and DARDAR above 2 km for almost all seasons. In December–February (DJF), when a vast majority of scenes are composed of semitransparent ice clouds, the agreement is even better. An exception happens in MAM when clouds were seen by EUREKA_G/B above 2 km and missed by DARDAR.

Downloaded from http://journals.ametsoc.org/jamc/article-pdf/53/11/2553/3577679/jamc-d-14-0021_1.pdf by guest on 19 November 2020

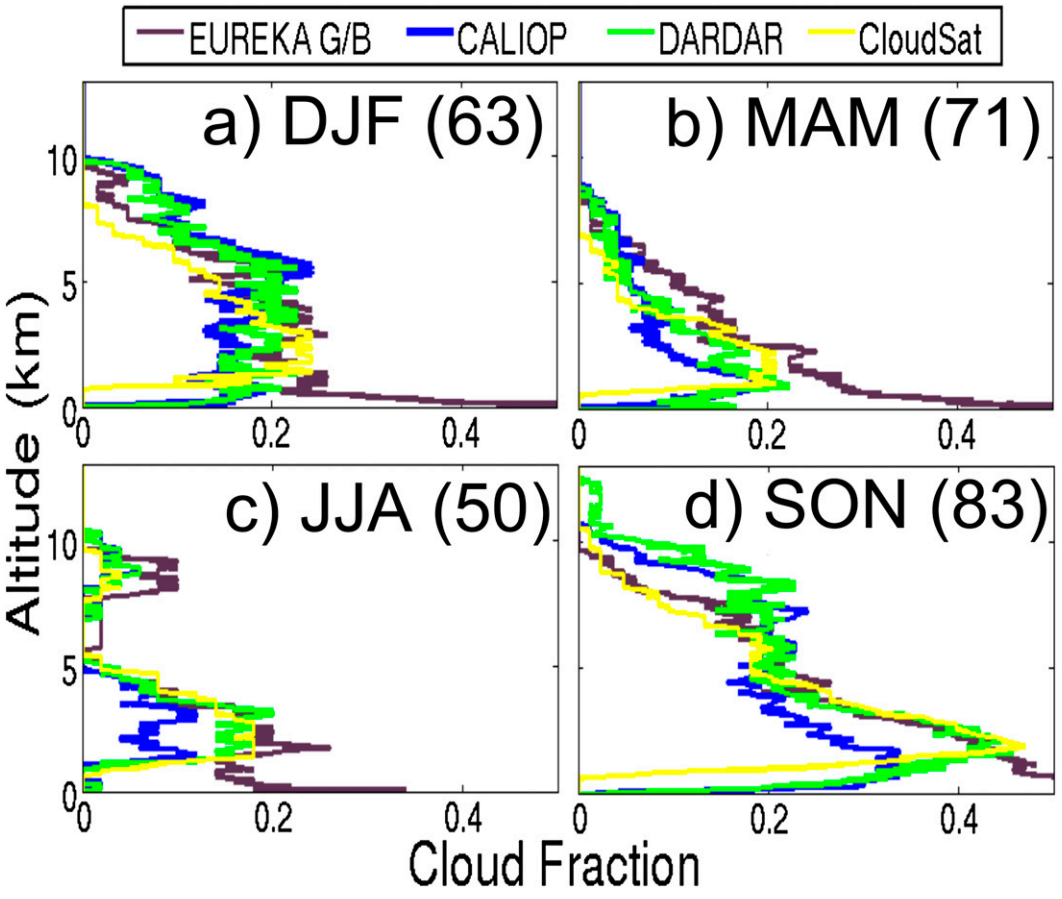

FIG. 6. As in Fig. 5, but for the (a) DJF, (b) MAM, (c) JJA, and (d) SON seasons. The number of profiles for each season is in parentheses.

This could be attributed to water clouds, but CALIOP and *CloudSat* appear to agree well. Furthermore, temperatures are cold, close to 233 K at 5 km where there are evidences of differences, indicating the presence of ice particles. A further analysis showed that the disparities are caused by ice-particle layers with very small optical depths (less than 0.08) that were not detected by the spaceborne lidar. Significant differences in CALIOP cloud frequency with respect to the other datasets are also seen below 4 km [CALIOP appearing to be negatively (low) biased], during summer and autumn periods when mixed-phase or liquid clouds are detected.

5. Discussion

In both independent- and coincident-observations analyses, EUREKA_G/B detects a majority of ice, aerosol particles, and liquid droplets, with few mixed-phase cases being present. In the independent data analysis (see Fig. 3a), the overall cumulated cloud fraction exceeds 0.3 up to almost 6 km. This latter value is well above the satellite cloud fractions derived from CALIOP, *Cloudsat*, and DARDAR. The coincident analysis confirms the particular behavior of the EUREKA_G/B cloud vertical profile only up to 2 km. In the boundary layer, the very high occurrence of atmospheric features is associated with the presence of ice crystals or diamond dusts (Bourdages et al. 2009; Shupe 2011) that are indeed captured very well by ground-based instruments. Meanwhile the detection of low-tropospheric ice crystals remains challenging for spaceborne instruments. The other disparities observed in the independent statistical analysis appear to be more frequently caused by instrumental failures, which lead to significant differences that are due to different time sampling. This result confirms that, as previously identified by Protat et al. (2006), sampling representativeness is a first prerequisite to reduce biases.

The analysis of coincident measurements of Arctic scenes from ground-based and spaceborne sensors shows that none of the instruments or observations can be interpreted as the ultimate truth, although lidar–radar

Downloaded from http://journals.ametsoc.org/jamc/article-pdf/53/11/2553/3577679/jamc-d-14-0021_1.pdf by guest on 19 November 2020

synergies show relatively good agreement between them above 2 km. This latter value is related to the geographical context of the Eureka station. Over this limit, the lidar–radar synergy appears to be essential to have the right picture of the vertical cloud distribution, as proposed by Protat et al. (2006) and Stein et al. (2011).

On the basis of our findings regarding the inherent instrumental and methodological limitations, we suggest a number of recommendations to be taken into account in any Arctic cloud study:

1) First, a coincident analysis should consider that the narrow field of view of active instruments may not allow us to measure the same atmospheric features as the ground-based station does. For instance, in our study, the hit rate was 95% for overpasses within 5 km of the station but decreased to 80% for overpasses farther than 20 km away. False detection happened mostly (86%) when A-Train overpasses were farther than 10 km away from the Eureka site.
2) Sensors' inner limits are still a major constraint in a study of cloud vertical profile. While the radar is not able to detect small particles and the lidar is incapable of seeing through opaque clouds, the synergy between the two instruments is still well suited for the detection and analysis of these scenes. In this study, however, only about 25% of the cloudy scenes are composed of opaque clouds, causing misdetections of small ice particle clouds of a few percent at high altitude. Meanwhile semitransparent cloud (optical depth < 3) vertical profiles can be fully retrieved, as shown in Fig. 6a. It is important to note that the cloud-detection method is different for each instrument used and depends on its performance and sensitivity limits. This can have an impact on the cloud fraction because cloud-detection thresholds are often somewhat subjective depending on the designer's requirements. A sensitivity study of the thresholds is beyond the scope of this paper, but it may explain some differences, especially for very thin ice clouds.
3) The mountains surrounding the Eureka station present a significant challenge for surface detection and therefore identification of low atmospheric features. Indeed, correct ground surface detection is a sensitive issue because of ground return identification and the horizontal averaging used in satellite products (e.g., CALIOP L2). Thus unexpected features can appear in the retrieved properties, such as a supercooled layer in DARDAR. Several issues also appear in the case of passive instruments (as discussed in section 2d), which cause an underestimation of cloud fraction in winter. This is partially due to the difficulty of detecting very thin clouds (optical depth < 0.1) over a frozen surface (Ackerman et al. 2008; Y. Liu et al. 2010).
4) Boundary layer events, composed of aerosols and/or precipitating ice crystals, are one of the principal challenges raised by the coincident data analysis of this work. The detection of such events mainly depends on the classification thresholds since the backscatter and the depolarization ratio of boundary ice crystals may vary depending on their orientation and optical depth. Further analysis is warranted to study the presence of ice crystals suspended in the boundary layer that are frequently observed over different Arctic stations during the winter period. Eureka is not the best site for such a study, however, because it can be subject to blowing-snow intrusions from surrounding mountains (Lesins et al. 2009) and can also suffer from local pollution produced by station chimney exhausts.

6. Conclusions

In this paper, we have compiled cloud fraction measured at the Eureka station in the high Arctic by satellite and ground-based instruments. The comparison of the independent datasets between 2006 and 2010 revealed some discrepancies in annual and seasonal variations. The winter-months conditions (lack of sunlight, cold surface temperatures, high albedo, and the presence of nonprecipitating ice crystals close to the ground) create difficulties for passive instruments and weather observations. Lidar and lidar–radar data showed a good correlation in terms of cloud fraction despite some biases linked to their detection method. We conclude that individual datasets cannot be used to evaluate the performance of different instruments and methods without introducing biases that can be large when similar sampling is not achieved. In this work, we also undertook a comparison between ground-based and spaceborne classifications of collocated scenes over Eureka. Between June 2006 and May 2010, 267 A-Train overpasses were studied in terms of cloud fraction and vertical distribution. The synergy lidar–radar appeared to be the only one to offer a complete picture of the cloud vertical profile, but it is limited to above 2 km. The misdetections below this altitude were mainly attributed to undetected low-level clouds because of the sensitivity loss induced by the attenuation of optically dense clouds for lidar and surface proximity for radar. The detection of precipitating low-tropospheric ice crystals from space is then complicated by the ground proximity and the mountainous terrain and requires further surface-based observations and active measurements.

Downloaded from http://journals.ametsoc.org/jamc/article-pdf/53/11/2553/3577679/jamc-d-14-0021_1.pdf by guest on 19 November 2020

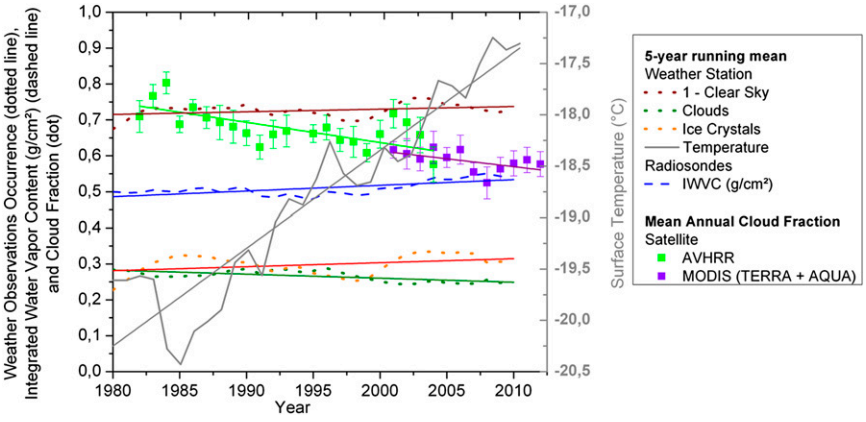

FIG. A1. Surface temperature (solid line), weather-observation occurrences of given conditions (dotted lines), and integrated water vapor content (dashed line) 5-yr running means measured at Eureka, along with linear best fits. Colored squares are used for the annual cloud fraction (with standard errors) measured over Eureka with AVHRR and MODIS.

Acknowledgments. Acknowledgments are due to CANDAC, SEARCH, and Environment Canada for their operational support as well as for the AHSRL, MMCR, radiosondes, and observation data at Eureka. The authors thank the *CALIPSO* team at the NASA Langley Research Center, the ICARE data Center in Lille (France), and the *CloudSat* team at Colorado State University for the availability of the level-2 data. This research was supported by the Centre National d'Etudes Spatiales (CNES).

APPENDIX A

Long-Term Trends

a. Meteorological station

Figure A1 shows the 5-yr running mean of surface temperature (irregular solid line), weather observations occurrences (dotted lines), and integrated water vapor content (IWVC) (dashed line) from 1980. The hourly surface temperature climatology (straight gray line in Fig. A1) shows an increasing trend of $\sim 0.90°C\,(10\,yr)^{-1}$ since 1972 [as shown by Lesins et al. (2010), extended until 2012]. This temperature increase is more prevalent in autumn and spring during solar illumination and sea ice transitions. Radiosonde data were used to analyze the IWVC (dashed line in blue in Fig. A1). It shows a permanent augmentation $[+0.02\,g\,cm^{-2}\ (10\,yr)^{-1}]$ forced by stronger increases during summer (from 1 to $1.2\,g\,cm^{-2}$) but slight variations during the rest of the year, as shown from the Modern-Era Retrospective Analysis for Research and Applications (MERRA) by Serreze et al. (2012). The summer water vapor increase may be due to the intensified evaporation of ice-free areas during the periods of continuous solar illumination. This is particularly relevant given that Eureka is located near the border of the September sea ice minimum extent and close to the warmer North Atlantic Ocean (Serreze and Barry 2011; Serreze et al. 2012). The surface temperature inversion is a common feature in the Arctic during winter (Serreze et al. 1992). Using vertical temperature profiles, we found that the temperature inversions below a 1.2-km altitude at Eureka occur at an annual average rate of 65%–85%. The rate of inversion occurrence in the winter is over 95%. A summer inversion layer, a few hundred meters thick, occurs up to 78% of the time, with a typical lapse rate of $15°C\,km^{-1}$. This temperature inversion layer is important for lower-tropospheric stability and tends to decouple the surface from the atmosphere (Serreze and Barry 2005). It can also affect infrared measurements from ground-based and spaceborne sensors when cloud base is hotter than the surface.

Hourly observations from the weather station were annually averaged. Results reported in Fig. A1 show that the frequency of "ice crystals" is between 0.23 and 0.35 since 1980, comparable to cloud fraction. Ice-crystal observations are predominant during the winter period (they occur 70%–90% of time) and are linked to lower-tropospheric mist events. Part of the increase may be attributed to fog caused by local pollution from exhaust and power generators. The total nebulosity expressed as TN = 1 − clear sky is between 0.68 and 0.75, with a trend of $+0.7\%\,(10\,yr)^{-1}$. These statistics seem to be questionable because of the lack of visibility during the winter season and the low cloud frequency. This 30-yr trend exhibits a small increase in non-clear-sky observations that is relatively small in comparison with trends over land observed in EW2010a. In a similar way, we find opposite trends in the spaceborne passive

Downloaded from http://journals.ametsoc.org/jamc/article-pdf/53/11/2553/3577679/jamc-d-14-0021_1.pdf by guest on 19 November 2020

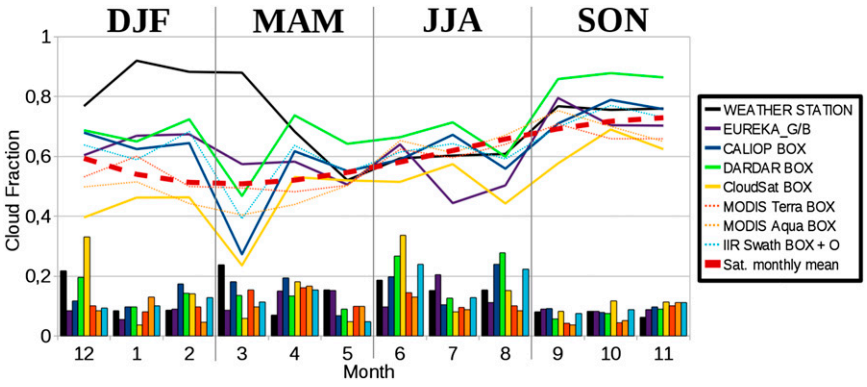

FIG. B1. Monthly cloud fraction for all of the datasets (weather station, EUREKA_G/B, CALIOP, DARDAR, *CloudSat*, MODIS, and IIR) corresponding to the seasonal variations reported in Table 2. The histograms of colored bars represent the standard deviations of each month related to each dataset. The dashed thick curve represents the best polynomial fit to the monthly mean of all satellite observations. The bars, showing one standard deviation, are relatively small and are driven by the interannual variations.

instruments when compared with the ground observations, emphasizing the need to go into further detail in the analysis.

b. Passive sensor satellites

In the current studies of cloud trends from space, only passive instruments provide more than 10 years of continuous estimates of cloud fraction. In Fig. A1 we use the passive AVHRR (from the Cooperative Institute for Meteorological Satellite Studies Internet site: http://stratus.ssec.wisc.edu/) and MODIS (both *Aqua* and *Terra* level-2 products, obtained online from http://modis-atmos.gsfc.nasa.gov/) data to look at cloud-fraction trends with respect to the one from surface observations. Figure A1 equally shows a 4-yr overlap for the two passive instruments where annual cloud fractions were similar (difference $< 10\%$) that may derive from the difference in time of overpasses and the cloud-detection method. The two passive instruments have negative cloudiness trends $[-2\%\,(10\,\mathrm{yr})^{-1}$ for AVHRR and $-4\%\,(10\,\mathrm{yr})^{-1}$ for MODIS] that are similar to some other Arctic studies [see EW2010a for AVHRR over land areas, Schweiger (2004), and Wang et al. (2012)].

APPENDIX B

Seasonal and Monthly Variations Considering Independent Datasets

This appendix is an extension of section 3b. According to Table 2, MODIS and *CloudSat* have consistently smaller values than the other datasets. This especially happens during DJF and MAM (including CALIOP also for this latter season) when the surface is cold and frozen and when cloud particles (often composed of ice) are generally smaller. DARDAR BOX shows the highest cloud fraction among satellite datasets for all seasons. As mentioned in section 3a, we saw that a significant part of this cloud fraction is driven by the first pixels above the ground. We estimated that this causes a positive bias of close to 10%, especially during winter and spring. DARDAR BOX HIGH removes misidentifications that are due to surface cluster (over a surface covered by snow) but may also sometimes miss real features. The difference between *CloudSat* BOX and *CloudSat* BOX 2 of about 5% is due to pixels having a cloud mask of 6–10. The false rate of detection of the pixels with a cloud mask of 6–10 is about 44% relative to *CALIPSO* cloud products, however (Marchand et al. 2008). In winter, CALIOP BOX detects almost the same amount of clouds as DARDAR BOX ALL does, but a part of those are clouds close to the snow-covered surface. IIR SWATH BOX + O is comparable to CALIOP BOX during all seasons and is even slightly larger in spring. The main difference is then due to the swath analysis, extending CALIOP measurements along the track.

To look at possible interactions between cloud-detection efficiency and ice surface, monthly cloud-fraction signature is a more suited parameter. It is expected that ice-free ocean surfaces have a flatter response than that over islands and land surfaces (EW2010b). Figure B1 shows the monthly-mean cloud fraction and its variability derived in this study.

For all of the datasets for the period 1 June 2006–31 May 2010, overall agreement between all space observations is observed (March excepted, see further). As previously discussed, weather-station data are much larger in winter and early spring (which is due to the

Downloaded from http://journals.ametsoc.org/jamc/article-pdf/53/11/2553/3577679/jamc-d-14-0021_1.pdf by guest on 19 November 2020

predominance of ice-crystal events, about 70%–90% of the winter observations). *CloudSat* and DARDAR are shown to be the two extreme datasets giving the smaller and the larger cloud fractions. Showing higher values during September–November (SON) and smaller values during MAM and June–August (JJA), it is similar to the land box variations in EW2010b, determined for a part of Siberia. These results are also consistent with those given for the Arctic regional average derived from the *CloudSat* geometric profile product (GEOPROF-2B) as reported in Kay and L'Ecuyer (2013), confirming a deficit of 0.15 for *CloudSat* relative to a combination of *CALIPSO* and *CloudSat* (as derived from DARDAR). All of the sensors detect a maximum of cloud fraction during autumn (SON values are larger than the values for the other seasons by ~0.12). Indeed, the minimum September sea ice extent and the decrease of surface temperatures can both lead to a transition between August and September with a marked increase in cloud fraction (EW2010b; Liu et al. 2012a). This has a strong impact on the surface energy budget (Sedlar et al. 2012). In March the shrinkage appears to be associated with a medium standard deviation, indicating a significant behavior. Although this decrease is seen by all A-Train instruments, except for MODIS because of area averaging, it is not observed at a larger scale (see, e.g., Fig. 1 in Liu et al. 2012a).

MODIS is less sensitive to very thin ice clouds [optical depth (OD) < 0.4] than is CALIOP (Ackerman et al. 2008). Therefore analysis of the monthly curves helps one to understand the limitations associated with the passive sensors. Despite the nighttime cloud-detection algorithm, MODIS underestimates cloud fraction during winter (from October to February). An analysis of OD retrieved from CALIOP (not shown here) displays a predominance of thin ice clouds (OD < 1) in the winter when the water vapor amount is smaller. Moreover, MODIS cloud detection also depends on the sea ice concentration and tends to underestimate the presence of clouds (Y. Liu et al. 2010). In summer the permanent solar illumination can cause a bias in CALIOP cloud detection (for thin clouds or at low levels where the vertical transmission is smaller) since daytime measurements have a lower signal-to-noise ratio than at night. During the summer and autumn periods, dominated by thick and opaque clouds (OD > 3), both instruments detect almost the same amount of cloud.

REFERENCES

Ackerman, S. A., R. E. Holz, R. Frey, E. W. Eloranta, B. C. Maddux, and M. McGill, 2008: Cloud detection with MODIS. Part II: Validation. *J. Atmos. Oceanic Technol.,* **25,** 1073–1086, doi:10.1175/2007JTECHA1053.1.

Beesley, J. A., 2000: Estimating the effect of clouds on the Arctic surface energy budget. *J. Geophys. Res.,* **105,** 10 103–10 117, doi:10.1029/2000JD900043.

——, and R. E. Moritz, 1999: Toward an explanation of the annual cycle of cloudiness over the Arctic Ocean. *J. Climate,* **12,** 395–415, doi:10.1175/1520-0442(1999)012<0395:TAEOTA>2.0.CO;2.

Bourdages, L., T. J. Duck, G. Lesins, J. R. Drummond, and E. W. Eloranta, 2009: Physical properties of high Arctic tropospheric particles during winter. *Atmos. Chem. Phys.,* **9,** 6881–6897, doi:10.5194/acp-9-6881-2009.

Chan, M. A., and J. C. Comiso, 2011: Cloud features detected by MODIS but not by *CloudSat* and CALIOP. *Geophys. Res. Lett.,* **38,** L24813, doi:10.1029/2011GL050063.

Comiso, J. C., 2012: Large decadal decline of the Arctic multiyear ice cover. *J. Climate,* **25,** 1176–1193, doi:10.1175/JCLI-D-11-00113.1.

Curry, J. A., J. L. Schramm, W. B. Rossow, and D. Randall, 1996: Overview of Arctic cloud and radiation characteristics. *J. Climate,* **9,** 1731–1764, doi:10.1175/1520-0442(1996)009<1731:OOACAR>2.0.CO;2.

Delanoë, J., and R. J. Hogan, 2008: A variational scheme for retrieving ice cloud properties from combined radar, lidar, and infrared radiometer. *J. Geophys. Res.,* **113,** D07204, doi:10.1029/2007JD009000.

——, and ——, 2010: Combined *CloudSat–CALIPSO*–MODIS retrievals of the properties of ice clouds. *J. Geophys. Res.,* **115,** D00H29, doi:10.1029/2009JD012346.

Di Pierro, M., L. Jaeglé, E. W. Eloranta, and S. Sharma, 2013: Spatial and seasonal distribution of Arctic aerosols observed by the CALIOP satellite instrument (2006–2012). *Atmos. Chem. Phys.,* **13,** 7075–7095, doi:10.5194/acp-13-7075-2013.

Dong, X., B. Xi, K. Crosby, C. N. Long, R. S. Stone, and M. D. Shupe, 2010: A 10 year climatology of Arctic cloud fraction and radiative forcing at Barrow, Alaska. *J. Geophys. Res.,* **115,** D17212, doi:10.1029/2009JD013489.

Donovan, D. P., and A. C. A. P. van Lammeren, 2001: Cloud effective particle size and water content profile retrievals using combined lidar and radar observations 1. Theory and examples. *J. Geophys. Res.,* **106,** 27 425–27 448, doi:10.1029/2001JD900243.

Eastman, R., and S. G. Warren, 2010a: Interannual variations of Arctic cloud types in relation to sea ice. *J. Climate,* **23,** 4216–4232, doi:10.1175/2010JCLI3492.1.

——, and ——, 2010b: Arctic cloud changes from surface and satellite observations. *J. Climate,* **23,** 4233–4242, doi:10.1175/2010JCLI3544.1.

Eloranta, E. W., 2005: High spectral resolution lidar. *LIDAR: Range-Resolved Optical Remote Sensing of the Atmosphere,* K. Weitkamp, Ed., Springer Series in Optical Sciences, Vol. 102, Springer, 143–163.

——, T. Uttal, and M. Shupe, 2007: Cloud particle size measurements in Arctic clouds using lidar and radar data. *Proc. Int. Geosci. Remote Sens. Symp. IGARSS 2007,* Barcelona, Spain, IEEE International, 2265–2267. [Available online at http://ieeexplore.ieee.org/xpl/articleDetails.jsp?arnumber=4423292.]

Garnier, A., J. Pelon, P. Dubuisson, M. Faivre, O. Chomette, N. Pascal, and D. P. Kratz, 2012: Retrieval of cloud properties using *CALIPSO* imaging infrared radiometer. Part I: Effective emissivity and optical depth. *J. Appl. Meteor. Climatol.,* **51,** 1407–1425, doi:10.1175/JAMC-D-11-0220.1.

Grenier, P., J.-P. Blanchet, and R. Muñoz Alpizar, 2009: Study of polar thin ice clouds and aerosols seen by *CloudSat* and

Downloaded from http://journals.ametsoc.org/jamc/article-pdf/53/11/2553/3577679/jamc-d-14-0021_1.pdf by guest on 19 November 2020

CALIPSO during midwinter 2007. *J. Geophys. Res.,* **114,** D09201, doi:10.1029/2008JD010927.

Hahn, C., S. Warren, and J. London, 1995: The effect of moonlight on observation of cloud cover at night, and application to cloud climatology. *J. Climate,* **8,** 1429–1446, doi:10.1175/1520-0442(1995)008<1429:TEOMOO>2.0.CO;2.

Intrieri, J., and M. Shupe, 2004: Characteristics and radiative effects of diamond dust over the western Arctic Ocean region. *J. Climate,* **17,** 2953–2960, doi:10.1175/1520-0442(2004)017<2953:CAREOD>2.0.CO;2.

Kahn, B. H., A. Eldering, A. J. Braverman, E. J. Fetzer, J. H. Jiang, E. Fishbein, and D. L. Wu, 2007: Toward the characterization of upper tropospheric clouds using Atmospheric Infrared Sounder and Microwave Limb Sounder observations. *J. Geophys. Res.,* **112,** D05202, doi:10.1029/2006JD007336.

Kay, J. E., and T. L'Ecuyer, 2013: Observational constraints on Arctic Ocean clouds and radiative fluxes during the early 21st century. *J. Geophys. Res. Atmos.,* **118,** 7219–7236, doi:10.1002/jgrd.50489.

——, ——, A. Gettelman, G. Stephens, and C. O'Dell, 2008: The contribution of cloud and radiation anomalies to the 2007 Arctic sea ice extent minimum. *Geophys. Res. Lett.,* **35,** L08503, doi:10.1029/2008GL033451.

Kim, S.-W., S. Berthier, J.-C. Raut, P. Chazette, F. Dulac, and S.-C. Yoon, 2008: Validation of aerosol and cloud layer structures from the space-borne lidar CALIOP using a ground-based lidar in Seoul, Korea. *Atmos. Chem. Phys.,* **8,** 3705–3720, doi:10.5194/acp-8-3705-2008.

——, E.-S. Chung, S.-C. Yoon, B.-J. Sohn, and N. Sugimoto, 2011: Intercomparisons of cloud-top and cloud-base heights from ground-based lidar, *CloudSat* and *CALIPSO* measurements. *Int. J. Remote Sens.,* **32,** 1179–1197, doi:10.1080/01431160903527439.

Kovacs, T., and P. McCormick, 2005: *Cloud-Aerosol Lidar and Infrared Pathfinder Satellite Observations* (*CALIPSO*) quid pro quo validation plan. [Available online at http://calipsovalidation.hamptonu.edu/QPQ_plan062206.htm.]

Lesins, G., L. Bourdages, T. J. Duck, J. R. Drummond, E. W. Eloranta, and V. P. Walden, 2009: Large surface radiative forcing from topographic blowing snow residuals measured in the high Arctic at Eureka. *Atmos. Chem. Phys.,* **9,** 1847–1862, doi:10.5194/acp-9-1847-2009.

——, T. J. Duck, and J. R. Drummond, 2010: Climate trends at Eureka in the Canadian high Arctic. *Atmos.–Ocean,* **48,** 59–80, doi:10.3137/AO1103.2010.

Lhermitte, R., 1987: A 94-GHz Doppler radar for cloud observations. *J. Atmos. Oceanic Technol.,* **4,** 36–48, doi:10.1175/1520-0426(1987)004<0036:AGDRFC>2.0.CO;2.

Liu, Y., J. R. Key, R. A. Frey, S. A. Ackerman, and W. Menzel, 2004: Nighttime polar cloud detection with MODIS. *Remote Sens. Environ.,* **92,** 181–194, doi:10.1016/j.rse.2004.06.004.

——, S. A. Ackerman, B. C. Maddux, J. R. Key, and R. A. Frey, 2010: Errors in cloud detection over the Arctic using a satellite imager and implications for observing feedback mechanisms. *J. Climate,* **23,** 1894–1907, doi:10.1175/2009JCLI3386.1.

——, J. R. Key, S. A. Ackerman, G. G. Mace, and Q. Zhang, 2012a: Arctic cloud macrophysical characteristics from *CloudSat* and *CALIPSO*. *Remote Sens. Environ.,* **124,** 159–173, doi:10.1016/j.rse.2012.05.006.

——, ——, Z. Liu, X. Wang, and S. J. Vavrus, 2012b: A cloudier Arctic expected with diminishing sea ice. *Geophys. Res. Lett.,* **39,** L05705, doi:10.1029/2012GL051251.

Liu, Z., R. Marchand, and T. Ackerman, 2010: A comparison of observations in the tropical western Pacific from ground-based and satellite millimeter-wavelength cloud radars. *J. Geophys. Res.,* **115,** D24206, doi:10.1029/2009JD013575.

Lubin, D., and E. Morrow, 1998: Evaluation of an AVHRR cloud detection and classification method over the central Arctic Ocean. *J. Appl. Meteor.,* **37,** 166–183, doi:10.1175/1520-0450(1998)037<0166:EOAACD>2.0.CO;2.

Marchand, R., G. G. Mace, T. Ackerman, and G. Stephens, 2008: Hydrometeor detection using *CloudSat*—An Earth-orbiting 94-GHz cloud radar. *J. Atmos. Oceanic Technol.,* **25,** 519–533, doi:10.1175/2007JTECHA1006.1.

McBean, G., and Coauthors, 2005: Arctic climate: Past and present. Arctic Climate Impact Assessment Scientific Rep., Cambridge University Press, 21–60. [Available online at http://www.acia.uaf.edu/PDFs/ACIA_Science_Chapters_Final/ACIA_Ch02_Final.pdf.]

Moran, K. P., B. E. Martner, M. J. Post, R. A. Kropfli, D. C. Welsh, and K. B. Widener, 1998: An unattended cloud-profiling radar for use in climate research. *Bull. Amer. Meteor. Soc.,* **79,** 443–455, doi:10.1175/1520-0477(1998)079<0443:AUCPRF>2.0.CO;2.

Platnick, S., M. King, S. Ackerman, W. Menzel, B. Baum, J. Riedi, and R. Frey, 2003: The MODIS cloud products: Algorithms and examples from *Terra*. *IEEE Trans. Geosci. Remote Sens.,* **41,** 459–473, doi:10.1109/TGRS.2002.808301.

Protat, A., A. Armstrong, M. Haeffelin, Y. Morille, J. Pelon, J. Delanoë, and D. Bouniol, 2006: Impact of conditional sampling and instrumental limitations on the statistics of cloud properties derived from cloud radar and lidar at SIRTA. *Geophys. Res. Lett.,* **33,** L11805, doi:10.1029/2005GL025340.

——, and Coauthors, 2009: Assessment of *CloudSat* reflectivity measurements and ice cloud properties using ground-based and airborne cloud radar observations. *J. Atmos. Oceanic Technol.,* **26,** 1717–1741, doi:10.1175/2009JTECHA1246.1.

Rigor, I., R. Colony, and S. Martin, 2000: Variations in surface air temperature observations in the Arctic, 1979–97. *J. Climate,* **13,** 896–914, doi:10.1175/1520-0442(2000)013<0896:VISATO>2.0.CO;2.

Rinke, A., C. Melsheimer, K. Dethloff, and G. Heygster, 2009: Arctic total water vapor: Comparison of regional climate simulations with observations, and simulated decadal trends. *J. Hydrometeor.,* **10,** 113–129, doi:10.1175/2008JHM970.1.

Rossow, W. B., and R. A. Schiffer, 1991: ISCCP cloud data products. *Bull. Amer. Meteor. Soc.,* **72,** 2–20, doi:10.1175/1520-0477(1991)072<0002:ICDP>2.0.CO;2.

Schweiger, A. J., 2004: Changes in seasonal cloud cover over the Arctic seas from satellite and surface observations. *Geophys. Res. Lett.,* **31,** L12207, doi:10.1029/2004GL020067.

——, R. W. Lindsay, S. Vavrus, and J. A. Francis, 2008: Relationships between Arctic sea ice and clouds during autumn. *J. Climate,* **21,** 4799–4810, doi:10.1175/2008JCLI2156.1.

Screen, J. A., C. Deser, and I. Simmonds, 2012: Local and remote controls on observed Arctic warming. *Geophys. Res. Lett.,* **39,** L10709, doi:10.1029/2012GL051598.

Sedlar, J., M. D. Shupe, and M. Tjernström, 2012: On the relationship between thermodynamic structure and cloud top, and its climate significance in the Arctic. *J. Climate,* **25,** 2374–2393, doi:10.1175/JCLI-D-11-00186.1.

Serreze, M. C., and R. G. Barry, 2005: *The Arctic Climate System.* Cambridge University Press, 385 pp.

——, and ——, 2011: Processes and impacts of Arctic amplification: A research synthesis. *Global Planet. Change,* **77,** 85–96, doi:10.1016/j.gloplacha.2011.03.004.

——, J. D. Kahl, and R. C. Schnell, 1992: Low-level temperature inversions of the Eurasian Arctic and comparisons with Soviet

Downloaded from http://journals.ametsoc.org/jamc/article-pdf/53/11/2553/3577679/jamc-d-14-0021_1.pdf by guest on 19 November 2020

drifting station data. *J. Climate,* **5,** 615–629, doi:10.1175/1520-0442(1992)005<0615:LLTIOT>2.0.CO;2.

——, A. P. Barrett, and J. Stroeve, 2012: Recent changes in tropospheric water vapor over the Arctic as assessed from radiosondes and atmospheric reanalyses. *J. Geophys. Res.,* **117,** D10104, doi:10.1029/2011JD017421.

Shupe, M. D., 2007: A ground-based multisensor cloud phase classifier. *Geophys. Res. Lett.,* **34,** L22809, doi:10.1029/2007GL031008.

——, 2011: Clouds at Arctic atmospheric observatories. Part II: Thermodynamic phase characteristics. *J. Appl. Meteor. Climatol.,* **50,** 645–661, doi:10.1175/2010JAMC2468.1.

——, and J. M. Intrieri, 2004: Cloud radiative forcing of the Arctic surface: The influence of cloud properties, surface albedo, and solar zenith angle. *J. Climate,* **17,** 616–628, doi:10.1175/1520-0442(2004)017<0616:CRFOTA>2.0.CO;2.

——, V. P. Walden, E. Eloranta, T. Uttal, J. R. Campbell, S. M. Starkweather, and M. Shiobara, 2011: Clouds at Arctic atmospheric observatories. Part I: Occurrence and macrophysical properties. *J. Appl. Meteor. Climatol.,* **50,** 626–644, doi:10.1175/2010JAMC2467.1.

Stein, T. H. M., J. Delanoë, and R. J. Hogan, 2011: A comparison among four different retrieval methods for ice-cloud properties using data from *CloudSat, CALIPSO,* and MODIS. *J. Appl. Meteor. Climatol.,* **50,** 1952–1969, doi:10.1175/2011JAMC2646.1.

Stephens, G. L., and Coauthors, 2002: The *CloudSat* mission and the A-Train. *Bull. Amer. Meteor. Soc.,* **83,** 1771–1790, doi:10.1175/BAMS-83-12-1771.

Stocker, T. F., and Coauthors, 2013: *Climate Change 2013: The Physical Science Basis.* Cambridge University Press, 1535 pp.

Tanelli, S., S. L. Durden, E. Im, K. S. Pak, D. G. Reinke, P. Partain, J. M. Haynes, and R. T. Marchand, 2008: *CloudSat*'s cloud profiling radar after two years in orbit: Performance, calibration, and processing. *IEEE Trans. Geosci. Remote Sens.,* **46,** 3560–3573, doi:10.1109/TGRS.2008.2002030.

Turner, D. D., S. A. Clough, J. C. Liljegren, E. E. Clothiaux, K. E. Cady-Pereira, and K. L. Gaustad, 2007: Retrieving liquid water path and precipitable water vapor from the Atmospheric Radiation Measurement (ARM) microwave radiometers. *IEEE Trans. Geosci. Remote Sens.,* **45,** 3680–3690, doi:10.1109/TGRS.2007.903703.

Vaughan, M. A., and Coauthors, 2009: Fully automated detection of cloud and aerosol layers in the *CALIPSO* lidar measurements. *J. Atmos. Oceanic Technol.,* **26,** 2034–2050, doi:10.1175/2009JTECHA1228.1.

Wang, X., and J. Key, 2005: Arctic surface, cloud, and radiation properties based on the AVHRR Polar Pathfinder dataset. Part II: Recent trends. *J. Climate,* **18,** 2575–2593, doi:10.1175/JCLI3439.1.

——, ——, Y. Liu, C. Fowler, J. Maslanik, and M. Tschudi, 2012: Arctic climate variability and trends from satellite observations. *Adv. Meteor.,* **2012,** 505613, doi:10.1155/2012/505613.

Winker, D. M., J. R. Pelon, and M. P. McCormick, 2003: The *CALIPSO* mission: Spaceborne lidar for observation of aerosols and clouds. *Lidar Remote Sensing for Industry and Environment Monitoring III,* U. N. Singh, T. Itabe, and Z. Liu, Eds., International Society for Optical Engineering (SPIE Proceedings, Vol. 4893), 1–11, doi:10.1117/12.466539.

——, M. A. Vaughan, A. Omar, Y. Hu, K. A. Powell, Z. Liu, W. H. Hunt, and S. A. Young, 2009: Overview of the *CALIPSO* mission and CALIOP data processing algorithms. *J. Atmos. Oceanic Technol.,* **26,** 2310–2323, doi:10.1175/2009JTECHA1281.1.

Downloaded from http://journals.ametsoc.org/jamc/article-pdf/53/11/2553/3577679/jamc-d-14-0021_1.pdf by guest on 19 November 2020